Available online at www.sciencedirect.com

ScienceDirect

journal homepage: www.elsevier.com/locate/he

Systematic thermodynamic approach for designing mixed refrigerants used in hydrogen precooling process

Ahmad K. Sleiti[*], *Wahib A. Al-Ammari*

Department of Mechanical & Industrial Engineering, College of Engineering, Qatar University, Doha, Qatar

HIGHLIGHTS

- First systematic thermodynamic approach to optimally design HPP mixed-refrigerants.
- Specific energy consumption (SEC) is remarkably 78.81% lower than existing HPP.
- For optimized SEC ethylene, H2, R14 instead of ethane, neon, NH_3 are recommended.
- Eight-component MRs achieve best optimal mixtures for cryogenic cooling processes.
- Seven-component MRs achieve superior SEC and compactness of heat exchangers.

GRAPHICAL ABSTRACT

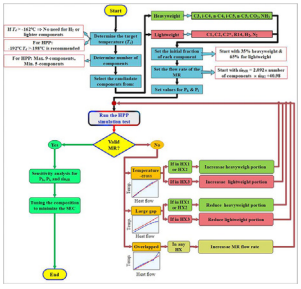

ARTICLE INFO

Article history:
Received 4 March 2022
Received in revised form
9 April 2022
Accepted 22 April 2022
Available online 18 May 2022

Keywords:
Hydrogen precooling process
H_2 liquefaction
Mixed refrigerants
Cryogenic refrigeration
Refrigerant selection

ABSTRACT

Designing an optimal mixed-refrigerant (MR) composition for any cryogenic refrigeration process plays a key role in the process overall performance. However, the existing approaches of developing mixed-refrigerants for these processes are difficult, time-consuming, and semi-random trial and error approaches. Therefore, for the first time, this study presents a systematic thermodynamic approach to optimally design mixed-refrigerants for any cryogenic process. In particular, the developed approach is conducted for the hydrogen precooling process (HPP) with a precooling temperature less than −193 °C. This approach consists of four criteria and seven major steps needed for the development of an energy-efficient HPP. Using this approach, 15 new mixed-refrigerants are created, analyzed, and compared based on the specific energy consumption (SEC) and coefficient of performance of the HPP. Further sensitivity analyses for the major operating conditions of the HPP are conducted for the best five cases. A minimum SEC of 1.03 kWh/khH2$_{Feed}$ at wet-cooling conditions and of 1.32 kWh/khH2$_{Feed}$ at dry-cooling conditions are achieved, which is remarkably 78.81% lower than the SEC of the existing HPP in commercial plants. This study also found that eight-component MR is the best

* *Corresponding author.*
E-mail address: asleiti@qu.edu.qa (A.K. Sleiti).

https://doi.org/10.1016/j.ijhydene.2022.04.233

option to create optimal mixtures for cryogenic cooling processes with perfect match between the composite curves of all heat exchangers of the HPP. While methane, nitrogen, and hydrogen components are essential for the MR to achieve energy-efficient HPP, the use of ethylene instead of ethane, H_2 instead of neon, and R14 instead of NH_3 is recommended to optimize the SEC.

Nomenclature

Symbol	*Description, (unit)*
COP	Coefficient of performance, (–)
$\dot{m}_{MR}$	Mass flow rate of the mixed refrigerant, (kg/s)
P_h	High-pressure of the precooling process, (bar)
P_l	Low-pressure of the precooling process, (bar)
P_{im}	Intermediate pressure of the compression process, (bar)
Q_{HX}	Cold duty of the heat exchanger, (MW)
$\dot{W}_{Com}$	Compression power of a compressor, (MW)
SEC	Specific energy consumption, (kWh/kgH2$_{Feed}$)
T_b	Boiling-point temperature of a component, (°C)
T_f	Freezing-point temperature of a component, (°C)
T_4	Target temperature of the precooling process, (°C)

Abbreviations

CL1, CL2 Cooler 1 and cooler 2
Com-1, Com-2 Compressor 1 and compressor 2
EV1, .., EV3 Expansion valve 1, .., expansion valve 3
GWP Global warming potential
HLP Hydrogen liquefaction process
HPP Hydrogen precooling process
HX1,.., HX3 Heat exchanger 1, .., heat exchanger 3
HSCN Hydrogen supply chain network
MR Mixed refrigerants
MSHXs Multi-stream heat exchanger
M1, .., M3 Mixer 1, .., mixer 2
S1, .., S3 Separator 1, .., separator 2

Introduction

Hydrogen is considered as the fuel of the future that will play a major role in the decarbonization of energy supplies and in integration of renewable energy systems [1]. Thus, recently, numerous research related to the different stages of the hydrogen supply chain network (HSCN: production [2], conditioning [3], transportation [4], and distribution [5]) were introduced. At large-scale, the hydrogen liquefaction process (HLP) is a key part of the HSCN from a technical and economical point of view [6]. In particular, hydrogen liquefaction is the best solution to transport large quantities over extended distances in a cost-effective way [7]. Also, it offers a low-pressure, high-energy density fuel to be used in a variety of applications [8]. However, the HLP is a very energy-intensive process [9], which forms a major barrier to its large-scale commercialization [10]. For instance, the specific energy consumption (SEC) of the most current operating large-scale hydrogen liquefaction plants lies in the range of 13–15 kWh/kg$_{LH2}$ [11]. This is much higher than even the least efficient natural gas liquefaction processes, which have a SEC of around 0.24 kWh/kg$_{LNG}$ [12]. Therefore, extensive research efforts have been devoted to achieving significant reduction in the SEC of the HLP as an essential step towards the economic feasibility of the HSCN [13,14].

On one hand, several concepts were introduced to minimize the electricity consumption in the overall liquefaction process by its integration with other energy systems such as organic Rankine cycle [15], absorption-based [16] or ejector-based [17] refrigeration systems, Solid oxide electrolyzer [18], and Kalina cycle [19]. However, these integrated systems increase the capital investment of the plant and suffer from low operating reliability. On the other hand, the hydrogen precooling process (HPP) has more degrees of freedom in the design and consumes more than 30% of the total consumed power by the hydrogen liquefaction plant. Therefore, several efforts were devoted to reduce the SEC of the hydrogen precooling process (HPP) by developing more efficient refrigerants [20], introducing innovative designs and process structures [21,22], and integrating the HPP with liquefied natural gas plants [23].

From a thorough review of the literature, it is found that the major HPPs can be categorized as: (a) nitrogen precooled cycles [24,25], (b) helium precooled cycles [26,27], (c) liquefied natural gas (LNG) precooled cycles [23,25,28,29], (d) Joule-Brayton (J-B) precooled cycles [21], (e) Joule-Thomson precooled cycles [30], and (f) mixed refrigerant (MR) precooled cycles [31–35]. As reviewed by Liang and Yonglin [21], the average specific energy consumption (SEC) of the nitrogen and helium precooled cycles is 11.47 kWh/kg$_{LH2}$ which is 76% higher than the J-B cycles (6.51 kWh/kg$_{LH2}$), and 89% higher than the MR precooled cycles (6.06 kWh/kg$_{LH2}$). This mainly caused by the need for a liquid nitrogen or helium to perform the precooling process, which need extra plant to cool and liquefy them. For the LNG precooled cycle, the SEC was 4.00 kWh/kg$_{LH2}$, which is the lowest value of all precooled technologies. However, this value excludes the consumed energy to liquefy the natural gas itself. In addition, the availability of LNG to perform the liquefaction process is not always feasible and the use of LNG limits the precooling temperature to less than −162 °C. In contrasts, the MR

precooled cycles precool the hydrogen feed gas and the mixed refrigerants with minimal compression power and the precooling process could reach to a temperature of −198 °C.

Utilizing the mixed-refrigerants (MR) for the HPP successfully reduces the SEC of the HLP to the range of 5–8 kWh/kg_{LH2} compared to 10–13 for nitrogen-based cycles, and 7–9 kWh/kg_{LH2} for J-B or J-T-based cycles [21]. This implies that the MR-based cycles reduce the SEC by an average of 33% enjoying the simplest configuration and largest capacities over the other proposed cycles. Although the MR-based precooling processes have superior performance compared to the other aforementioned processes, their SEC is still very high in comparison to those used in the liquefied natural gas technologies. By careful examination of the proposed MR-based precooling processes available in the literature, it can be noted that their high SEC is mainly caused by one or more of the following factors:

(1) Inappropriate selection of the single components of the refrigerant mixture. That means at least one of the selected components should not necessarily be included in the mixture. For instance, the presence of "Neon" instead of "hydrogen" in MR composition proposed by Berstad et al. [36] yields SEC of 2.051 kWh/$kgH2_{Feed}$, which is about two times higher than the SEC in case of using "hydrogen" (1.082 kWh/$kgH2_{Feed}$) as conducted by Sadaghiani and Mehrpooya [37]. Another example, the MR proposed by Asadnia and Mehrpooya in Ref. [34] contains 11 components with unnecessary existence for the "Propene" and "Ammonia" that form 14.31% of the mixture (molar-based). These components cause poor performance for the multi-stream heat exchangers (MSHXs) of the HPP as evidenced by their composite curves with SEC of 1.588 kWh/$kgH2_{Feed}$.
(2) Inappropriate proportions between the components of the refrigerant mixture. That means the selected components are right, however, their proportions yield either a very light or a very heavy mixture. In both cases, the resulted poor composite curves mean that higher refrigerant flow is needed, which maximizes the SEC of the HPP. For example, the five-component mixture presented by Krasae-in Ref. [33] is mainly composed of lightweight components (74%) with an excess portion for the hydrogen (4%), which causes large consumption of the compression power with SEC of 1.416 kWh/$kgH2_{Feed}$. In contrast, the heavy components in the nine-component mixture proposed by Ghorbani et al. [32] form about 55% of the mixture, which causes a large gap between the hot and cold composite curves of the MSHXs that operate at the first two stages of the HPP with SEC of 1.113 kWh/$kgH2_{Feed}$.
(3) Inappropriate determination of the suitable operating conditions of the HPP. In some studies, the selection and proportions of the mixture components are adequately perfect, but the operating pressure of the HPP (such as the high-pressure and low-pressure of the process) were not the best conditions for the used compositions. This returns to the lack of robust sensitivity analysis over a wide range of the operating conditions and the absence of the sensitivity analysis for component portions in the mixture. For example, the nine-component mixture introduced by Sadaghiani and Mehrpooya [37] yields better composite curves than of the aforementioned studies with SEC of 1.082 kWh/$kgH2_{Feed}$. However, the sensitivity analysis for the operating conditions and mixture composition was only conducted for the liquefaction part rather than the precooling part of the overall hydrogen liquefaction process, which could bring lower SEC as will be demonstrated later in this study.

The major reason for these factors is that the determination of the MR composition is a difficult and time-consuming step as it depends on a semi-random trial and error approach. There is no work available in the literature that provides prioritization guidelines for the MR component selection. In addition, there is no systematic approach on how to adjust the proportions of the selected components to achieve the optimal MR composition for the HPP. Therefore, the main objectives of the present study are:

- presenting principal thermodynamic guidelines for the selection of the MR components with a particular focus on the HPP. This is done by investigating the relationship between the thermodynamic properties of the selected components and their effect on the performance of the MSHXs of the HPP. The importance of this part is to avoid the selection of unnecessary components that yield higher SEC with no significant improvement on the performance of the MSHXs.
- developing systematic procedures to adjust the proportions of the selected components based on the results of the aforementioned thermodynamic investigation.
- creating new MR compositions for the HPP (by applying the developed systematic approach), which yield lower SEC than those available in the literature. Further sensitivity analysis is conducted to optimize the performance of the best new mixed refrigerants with a detailed comparison with the best compositions available in the literature.

The next four sections describe the configuration of the MR-based HPP (Section Description of the mixed-refrigerant hydrogen precooling process), the methodology of the study (Section Methodology), the results and discussion, and the main finding of this study (Section Conclusions).

Description of the mixed-refrigerant hydrogen precooling process

The hydrogen precooling process (HPP) refers to the process of cooling the hydrogen gas from ambient temperature to a precooled temperature (refers to as a target temperature in this study) of −193 °C at which equilibrium phase of ortho-para hydrogen gas form is achieved [38]. It is worth mentioning that the target temperature (T_4) depends on the method of the precooling process as well as on the composition of the MR in the case of MR-based HPP. For instance, in the hydrogen liquefaction system proposed by Bian et al. [23], the target temperature was −156 °C as it uses liquefied natural gas

(LNG) for the HPP. In the CO_2-based precooling hydrogen liquefaction process, the target temperature was −160 °C as the composition of the MR contains no hydrogen or lighter components, which is necessary to reach temperatures less than the ortho-para equilibrium temperature (−193 °C). However, even if high volatile (very light) refrigerants exist in the mixture, their proportions must be sufficient to reach such very low temperatures as proved experimentally by Krasae-in et al. in Ref. [39].

The typical configuration of the HPP using mixed refrigerant is depicted in Fig. 1. The hydrogen stream is fed to the HPP at an ambient temperature of 25 °C and pressure of 21 bar with more than 75% as ortho-hydrogen. Then, it cools down to a temperature less than −193 °C through three MSHXs (HX1, HX2, and HX3). In this study, the target temperature (T_4) is set to −198 °C to increase the reliability on that the hydrogen gas reaches the equilibrium phase between ortho-to-para forms. For the cooling process, a single MR is compressed from low-pressure ($P_l = 2$ bar) to an intermediate pressure ($P_{im} = 7$ bar) through compressor 1 (Com-1). Then, the MR is cooled down to an aftercooler temperature of 25 °C (using wet water-coolers) or 37 °C (using dry air-cooler) in CL1. After that, the liquid and vapor phases of the MR are separated in S1, the vapor part is compressed in Com-2 and the liquid part is pumped to a high-pressure ($P_h > 16$ bar). The pressurized vapor stream (9) is cooled down again in CL2 and mixed with the pressurized stream leaving the pump using a mixed (M3). The pressurized MR splits again in S2 into vapor stream (14) and liquid stream (26). The vapor stream is passed through the first heat exchanger (HX1, 14–15) and separated again in S3. The final vapor-phase mixture (state 16) is passed through HX2 and HX3 and throttled through the expansion valve (EV3) to a pressure of 2 bar and performs evaporation process (cold duty of HX3) through the process 19–20. Similarly, the final liquid mixture (at state 21) passes through HX2 (21–22), expands through EV2 (22–23), and mixes with stream 20 in M2 to perform the evaporation process of HX2 (24–25). The liquid-phase mixture at state 26 passes through HX1 (26–27), expands through EV1 (27–28), and mixes with stream 25 in M1 to perform the evaporation process of HX1 and then the whole mixture is directed back to the inlet of Com-1 (29–5). In the present study, the temperature setting of the heat exchangers was defined such that HX1 cools the hydrogen stream to −45 °C, HX2 further cools it to −105 °C, and HX3 cools it to a target temperature (−195 °C).

Methodology

In this section, the methodology of the developed systematic approach for the selection and design of optimal MR components is introduced and the assumptions and performance indicators used to assist the results are described.

Process simulation

To evaluate the performance of the HPP under certain operating conditions with various MR compositions, two performance indicators were used including: (1) the specific energy consumption (SEC), and (2) the coefficient of performance (COP) of the HPP. To calculate these indicators and to test the validation of the developed MR compositions, the HPP is simulated using Aspen HYSYS for each composition. For the simulation process, the following assumptions were made:

- The adiabatic efficiencies of Com-1 and Com-2 are set equal to 90%.
- The MR is cooled down to an aftercooler temperature of 25 °C through each cooler (wet cooling conditions).
- The pressure drops through the coolers and heat exchangers are neglected.
- The hydrogen gas is fed to the process at a temperature of 25 °C, pressure of 21.0 bar, and precooled to −195 °C.
- Peng-Robinson equation of state is implemented to calculate the thermodynamic properties of all streams.

The SEC is calculated by dividing the net total compression power of the precooling process by the mass flow rate of the hydrogen feed as:

$$SEC = \frac{\dot{W}_{Com-1} + \dot{W}_{Com-2} + \dot{W}_{Pump}}{\dot{m}_{HF}} \quad (1)$$

where $\dot{W}_{Com-1}$, $\dot{W}_{Com-2}$, and $\dot{W}_{Pump}$ are the compression power consumed by Com-1, Comp-2, and Pump, respectively. The COP is defined as:

$$COP = \frac{Q_{HX1} + Q_{HX2} + Q_{HX3}}{\dot{W}_{Com-1} + \dot{W}_{Com-2} + \dot{W}_{Pump}} \quad (2)$$

where Q_{HX1}, Q_{HX2}, and Q_{HX3} are the cold duty of HX1, HX2, and HX3, respectively.

Selection of the mixed refrigerant components

From the available MR compositions used in the MR-based HPP, different five-components to eleven-components mixed refrigerants were found in open literature. The single components of these mixtures with the boiling point temperature (T_b), freezing point temperature (T_f), and the global warming potential (GWP) of each component are presented in Table 1. From an environmental point of view, all of these components are considered low-grade GWP components except R14, which is considered a high GWP element as it belongs to perfluorocarbon refrigerants. In addition, these components have zero ozone depletion potential (ODP) [40]. In this study, these components were divided into two categories: lightweight components (includes C1, C2, C2*, R14, N_2, and H_2), and heavyweight components (C3, i-C4, n-C4, i-C5, n-C5, CO_2, and NH_3). All of the lightweight components have boiling point temperatures less than −100 °C and freezing point temperatures lower than −168 °C, which make them responsible for providing the target temperature of the HPP and the cooling process through HX3. In contrast, the heavyweight components have boiling point temperature higher than −88 °C and freezing point temperature (except C3) higher than −160 °C, which make them responsible for the major specific refrigeration effect (cooling capacity) through HX1 and HX2.

After examining the available MR composition for the HPP process using Aspen HYSYS, it was found that the nine-component MR is sufficiently enough to obtain optimal

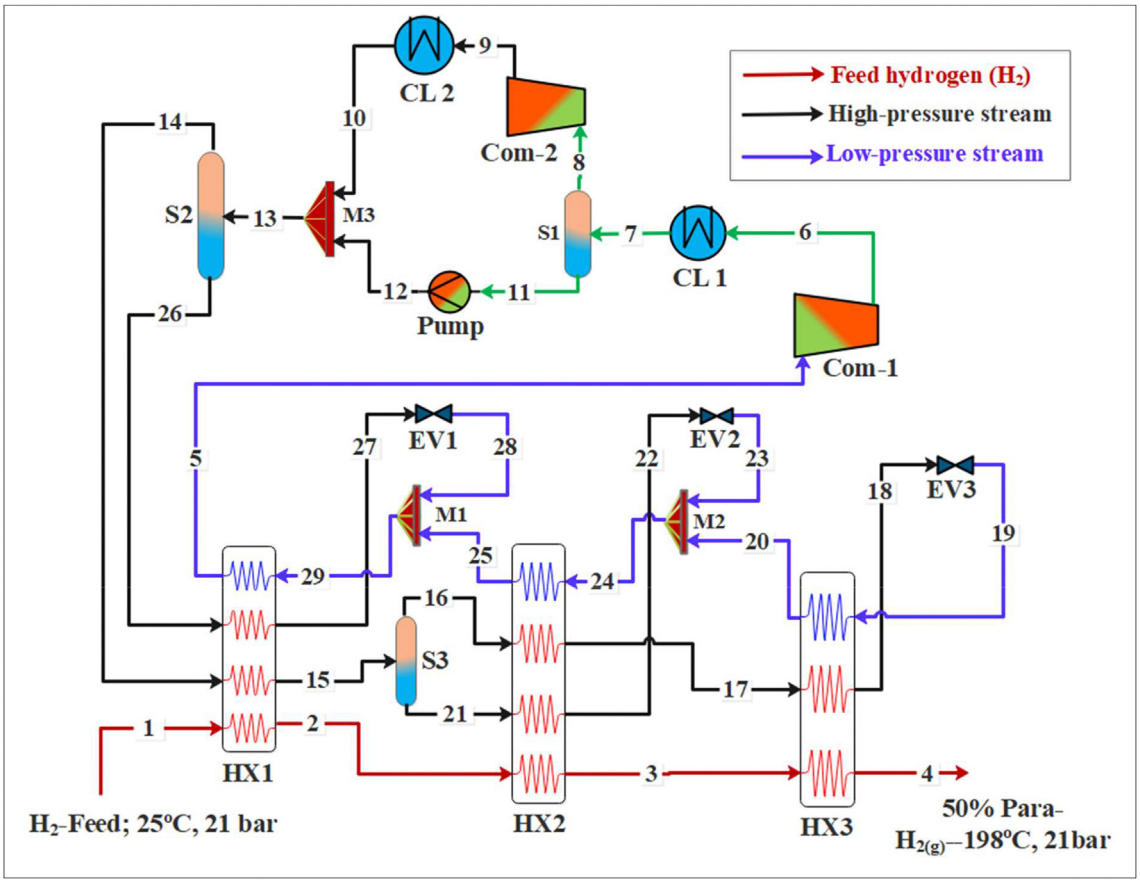

Fig. 1 – Process flow diagram of the MR-based hydrogen precooling process.

composite curves for all MSHXs in the HPP. A higher number of components leads to more compression power with no further improvement in the performance of the MSHXs. In contrast, four-component MR yields large temperature gaps in the composite curves of the MSHXs as it fails to smoothly match the hot composite curve of the feed hydrogen. This, in turn, increases the flow rate of the MR and thus the SEC of HPP. Therefore, it is concluded that the MR should contain no more than 9 components or less than 5 components for the HPP. In the present study, five groups of MRs were developed and compared to each other based on a systematic approach explained in the next section. These groups were distinguished based on the number of the single components in each MR; therefore, MR9, MR8, MR7, MR6, and MR5 denote the group with nine-, eight-, seven-, six-, and five-components MR, respectively. For each MR group, three different compositions were tested by either changing one or more of single components or just by changing their proportions. As a result, fifteen new mixed refrigerants (15 cases) for the HPP were systematically developed, tested, and analyzed in this study.

Among the six lightweight components, C1, N_2, and H_2 have boiling temperatures much lower than of C2, C2*, and R14, and thus they have more effect on the performance of HX3. For the HPP with a target temperature less than −193 °C, the presence of C1, N_2, and H_2 is essential and therefore they were considered in all cases of the present study.

Considering that C1, N_2, and H_2 (which are the lightest components) will exist in all cases, the other single components for each group will be selected based on the following four criteria (which are developed based on numerous simulation processes conducted in Aspen Hysys):

(a) For MR5: one heavy component is needed to serve in HX1 (such as C3, i-C4, n-C4, etc.) and one heavier component than methane and lighter than propane to serve in HX2 (such as C2, C2*, or R14).
(b) For MR6: similar to MR5 with heavier components to improve the composite curve of HX1 (as the existed lightweight components are enough to get optimal composite curves for HX3). However, as noted through the simulation process, the composite curve of HX2 will need further improvement.
(c) For MR7: one heavier component than methane and lighter than propane is needed to enhance the performance of HX2 (such as CO_2 and R14). It is found that seven components sufficiently provide optimal composite curves for the whole MSHXs in the HPP with minimal SEC. However, the proportions of the lightweight components can be reduced for further reduction in SEC by implementing the next term.
(d) For MR8 and MR9: other components heavier than methane can be added to ensure the suitable

Table 1 – Thermophysical properties of the pure components of candidate refrigerants [41].

Component	Boiling point temp. (T_b) [°C]	Freezing point temp. (T_f) [°C]	GWP [100 years-based]
Lightweight components			
Ethane (C2)	−88.59	−182.80	6
Ethylene (C2[a])	−103.80	−169.20	6
Refrig-14 (R14)	−127.90	−183.60	7390
Methane (C1)	−161.50	−182.50	25
Nitrogen (N_2)	−195.80	−210.00	0
Hydrogen (H_2)	−252.80	−259.20	5.8
Heavyweight components			
Carbon Dioxide (CO_2)	−87.84	−56.56	3
Propane (C3)	−42.10	−187.70	4
Ammonia (NH_3)	−33.33	−77.65	0
i-Butane (i-C4)	−11.68	−159.60	5
n-Butane (n-C4)	−0.53	−138.30	5
i-Pentane (i-C5)	27.85	−160.50	11
n-Pentane (n-C5)	35.87	−129.70	11

[a] At a temperature of 25 °C and pressure of 1 bar.

proportions between heavy and lightweight components that yield minimal SEC at a higher coefficient of performance (COP).

In the next section, the detailed procedures to develop an optimal mixed refrigerant composition for the HPP are explained taking the aforementioned criteria into account.

Developing optimal mixed refrigerant composition for hydrogen precooling process

As shown in Fig. 2, the systematic procedures to develop an optimal MR composition can be explained as follows:

(1) Select the target temperature of the precooling process. This is an essential step to exclude unnecessary components that cause either high compression power or freezing possibility through the cryogenic stages of the process. For instance, if the target temperature is less than −162 °C, there is no need for hydrogen or lighter components to be involved in the composition (see the MR compositions presented in Refs. [31,42]). In contrast, if the target temperature is lower than −193 °C, then the existence of very light components (such as hydrogen or neon) is necessary. From an energetic point of view, as concluded from the simulation process, the use of hydrogen is preferred instead of neon in the HPP.

(2) Determine the number of the single components that need to be mixed to develop the MR composition. In the LNG process, four- or five-component MR are sufficiently enough to achieve optimal MR composition with a target temperature of −162 °C for the entire liquefaction process. However, with a target temperature lower than −193 °C for the HPP, at least a five-component mixture is needed to achieve valid composition with reasonable SEC. on the other side, a nine-component mixture is more than enough to obtain optimal MR composition as will be explained further in Section Analysis of the selected refrigerants.

(3) Select the candidate components from the heavyweight and lightweight refrigerants taking into account the aforementioned criteria in Section Selection of the mixed refrigerant components.

(4) Start initializing the fraction of each component in the mixture with a total fraction percent of 35% for heavyweight and 65% for lightweight components. For the basic components C1, N_2, and H_2, start with initial fractions of 21%, 17%, and 1%, respectively. These initial fractions were recommended based on the simulation results of numerous iterations were performed through the development of the investigated cases in this study. Initializing the composition with these fractions is necessary to facilitate the iteration and to avoid the appearance of thermophysical problems such as temperature-cross or overlapping, which will be discussed in step (7). Also, it should be noted that the fraction of H_2 should not exceed 2% to prevent the avoidable increase in the SEC as explained further in Section Analysis of the selected refrigerants.

(5) Set the initial flow rate of the total MR stream. Using the data obtained from the developed 15 MR cases in this study, it is found that a close value for the optimal mass flow rate can be estimated using the following formula: $\dot{m}_{MR} = 2.092 \times Number\ of\ single\ components \times \dot{m}_{H2_{Feed}} + 40.98$. Comparison between the initial estimated values using this formula and the final optimal values of the MR flow rates is provided in Appendix A (Fig. A1). As shown in Fig. A1, for most cases, the initial estimated values are slightly higher than the final optimal values, which significantly reduce the time of estimation.

(6) Set the low-pressure (P_l) and the high-pressure (P_h) of the HPP. A low-pressure of 2 bar and a high-pressure of 20 bar are recommended as the initial set.

(7) Now, simulate the HPP to check if the developed MR is valid or not. Valid MR means that there is no thermophysical problem (no temperature-cross, no large gap, and no overlaps on the composite curves) on the operation of HX1, HX2, and HX3. If this is the case, then further sensitive analysis for the process pressures and MR flow rate will be needed to find their optimal values. After that, the proportions of the MR can be further tuned to reach the minimum SEC for that composition. However, if there is one or more of the physical problems, the following strategy can be applied:

(I) Temperature-cross: as shown in Fig. 3(a), temperature-cross means that the composite curve of the hot fluid crosses over the composite curve of the cold fluid. It can occur in any heat exchanger of the HPP. Also, it appears at the left-part (LP), middle-part (MP), and or right-part (RP) of the composite curves. If it occurs in the LP, then increase the portion of the lightest components that existed in the selected heat exchanger. For

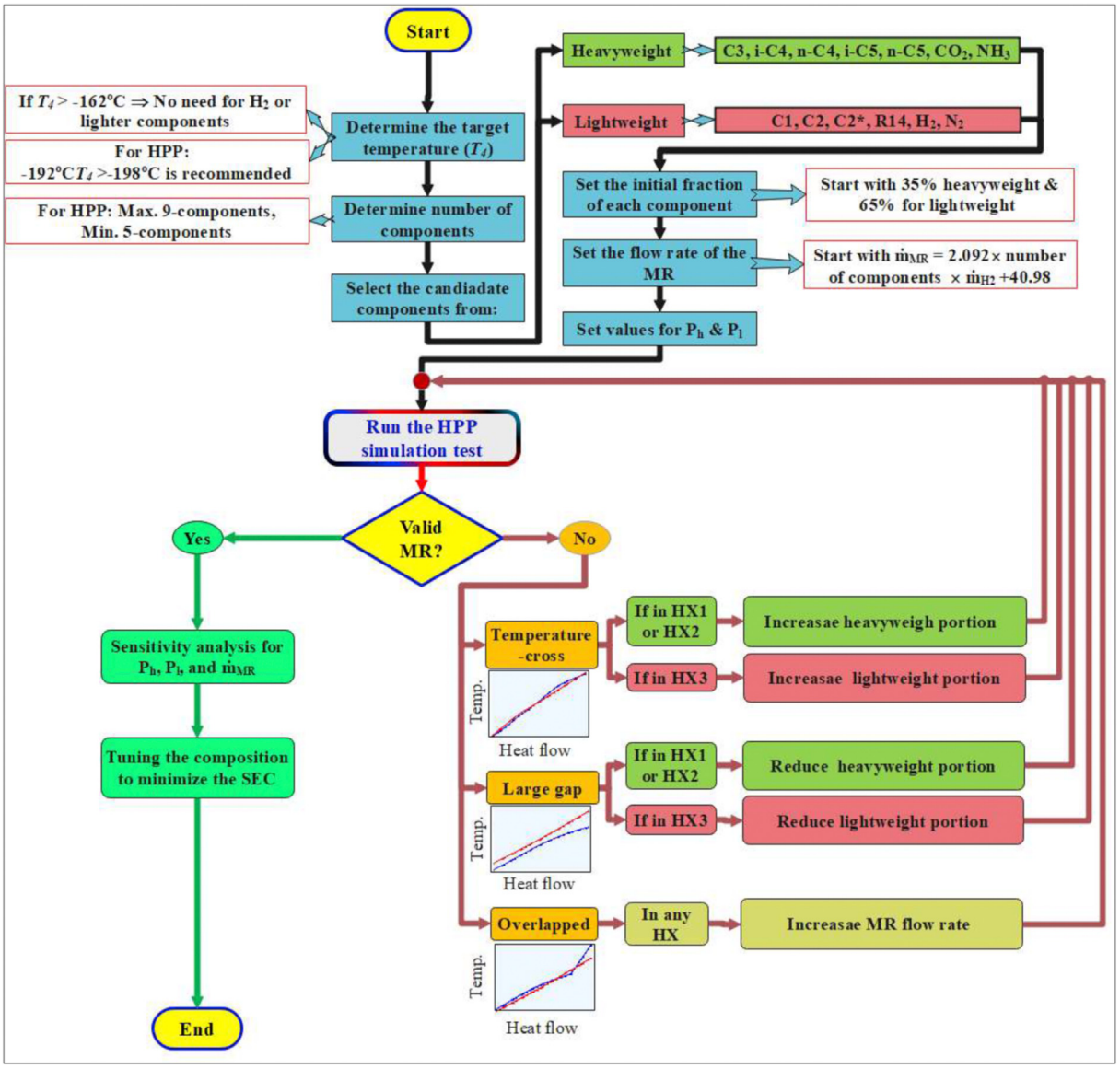

Fig. 2 – Systematic approach for the optimal development of mixed refrigerant composition for HPP.

instance, if it appears in the LP of HX3, increase the portion of H_2 and N_2 in the MR composition. If it appears in the RP section, increase the portion of the less lightweight components (e.x. increase the fraction of C2 or C2* if it appears in HX3). Similarly, if it appears in HX1 or HX2, increase the portion of the components assigned for that heat exchanger. In particular, increase the lighter component fractions for LP temperature-cross of heavier components fractions for RP or MP temperature-cross.

(II) Large-gap: as shown in Fig. 3(b), large-gap stands for the large temperature difference between the cold and hot composite curves. This issue is acceptable from a physical point of view, however, the large-gap increases the irreversibility of the process and consumes higher MR flow than necessary. Thus, to eliminate this issue, gradually reduce the MR flow until a minimum temperature approach limit is reached. In some cases, a smaller gap appears on LP than in MP or RP. If this is the case, then reduce the fractions of the components responsible for that MP and RP alongside the reduction of the total MR flow rate.

(III) Overlap: as shown in Fig. 3(c), overlap is a kind of temperature-cross, however, most of the cold composite curve is above the hot composite curve. As found through the simulation process, this problem was simply solved by increasing the MR flow rate, gradually.

Results and discussion

To ensure the validation of the selection criteria and design procedures for the development of an optimal MR composition, they were performed to develop 15 new MR compositions

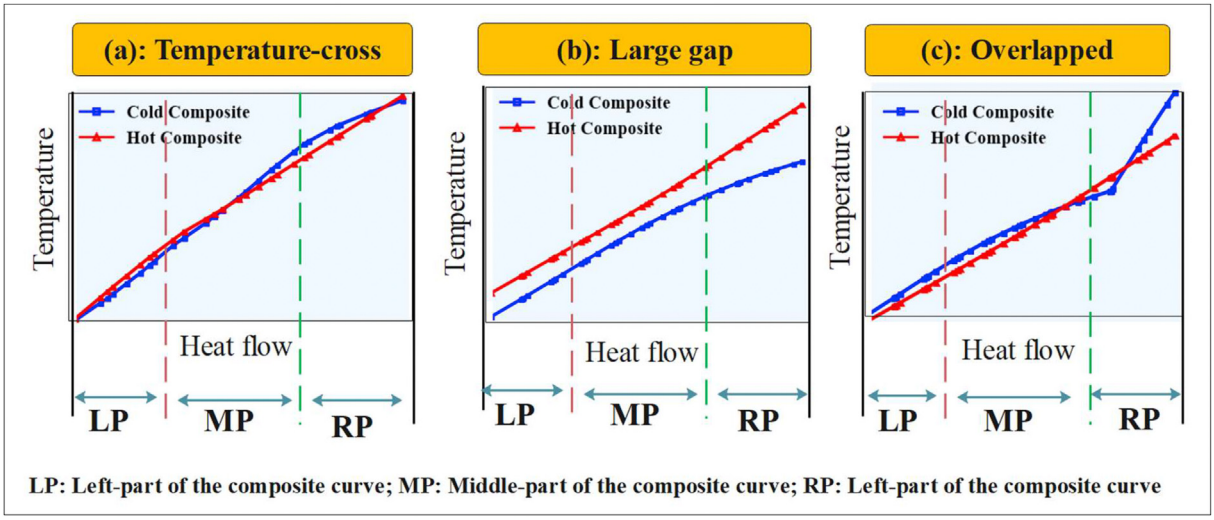

Fig. 3 – Thermophysical problems through the development process of an MR for the HPP. Note: in the presentation of this figure, the hot stream composed of pure hydrogen and the cold stream composed of a refrigerant mixture (C1, C2, C2*, C3, n-C4, n-C5, N_2, and H_2).

and their energetic performance was evaluated as detailed in Section Analysis of the selected refrigerants. In addition, sensitivity analyses for the operating conditions of the HPP and the composition of the best developed MR are conducted and discussed in Section Sensitivity analysis, and Section Composition sensitivity and comparisons, respectively.

Analysis of the selected refrigerants

The molar fractions of the 15 developed mixed refrigerants of this study are reported in Table 2. As mentioned above, these refrigerants were divided into five groups (MR5 to MR9) based on the number of the single components in each mixture. The total compression power and COP of the HPP for each MR are schematically presented in Fig. 4. The high-pressure (P_h), low-pressure (P_l), and MR flow rate ($\dot{m}_{MR}$) for each case are listed in Appendix A (Table A1). From Table 2, it is found that the lightweight component portions exceed 55% in each case with an average of 65% lightweight and 35% heavyweight components for all cases. In particular, the fractions of C1, N_2, and H_2 form at least 34% of the total composition for each case. Although the high portion of the lightweight components causes higher compression power, it is necessary to meet the refrigeration demand of the HPP at cryogenic temperatures. Also, it is more reliable to have no wet phase at the inlet of the first compressor (Com-1) that may damage it and negatively affect its lifetime. From the dramatic variations of the SEC and COP presented in Fig. 4, it can be stated that the nature of the composition and the proportions of the single components play a major role in the SEC of the HPP, as explained below.

Starting by considering the nature of the MR composition, it can be noted that Case 1 (MR9) has the maximum SEC of all cases (1.72 kWh/kgH2$_{Feed}$) which is higher than both Case 10 (MR6) and Case 13 (MR5) by an average of 8.4%. Although Case 1 contains nine components, which is a positive factor for a better match between the hot and cold composite curves of the MSHXs, the inclusion of NH_3 in the mixture causes a large gap at the right-part of the composite curves (See Fig. 5, Case 1) and requires MR flow of 143 kg/s, which is the highest flow of all cases. Replacing NH_3 by CO_2, as in Case 2, reduces the SEC to 1.34 kWh/kgH2$_{Feed}$ which is 22.2% lower than in Case 1. Similarly, replacing CO_2 by R14, as in Case 3, further reduces the SEC to 1.11 kWh/kgH2$_{Feed}$, which is 35.6% lower than of Case 1 and 17.3% lower than of Case 3. This is explained by that R14 has lower boiling point and freezing point temperatures than NH_3 and CO_2 which increase the refrigeration effect at a lower MR flow rate (98 kg/s in Case 3 compared to 143 kg/s in Case 1 and 112 kg/s in Case 2). In addition, the density of NH_3 at the outlet pressure of Com-1 (7 bar) and aftercooler temperature of 25 °C is 5.22 kg/m^3, which is lower than of CO_2 (12.89 kg/m^3) and R14 (25.48 kg/m^3) at the same conditions. This makes the density of Case 1(11.59 kg/m^3) lower than that of Case 2 (12.15 kg/m^3) and Case 3 (13.19 kg/m^3), which in turn further maximizes its compression power. Similar trends are noted for the replacement of NH_3 by CO_2 or R14 in MR8 and MR7 groups (Cases 4 to 6, and 7 to 9, respectively). In the last two groups MR6 and MR5, the portions of the lightweight components are higher than 64% and 76%, respectively. This makes the mixture more volatile and yields poor match for the composite curves as shown for Case 10 and Case 13 in Fig. 4. Therefore, the average SEC of MR6 and MR5 is 32% higher than that of MR7. This implies that the most efficient MR compositions (MR7) are obtained by removing unnecessary components such as NH_3 or CO_2 by avoiding the very high portions of lightweight components.

As the replacement of NH_3 by CO_2 or R14 yields a heavier mixture with lower SEC, the reduction of the number of single components allows the designer to modify the proportions of the components more accurately. For instance, unlike MR9 cases, the composition of MR7 cases has no C2 and n-C4 in the MR composition. The fractions of these components are substituted by increasing the fractions of C2* and C3. As C2* and C3 have boiling point temperatures lower than of C2 and n-C4, they increase the refrigeration effect of the mixture and

Table 2 – Molar fraction-based composition of the 15 mixed refrigerant cases.

Group	Case #	C1	C2	C2*	C3	n-C4	i-C5	n-C5	R14	N_2	H_2	CO_2	NH_3
MR9	1	0.17	0.07	0.16	0.18	0.02	0.00	0.15	0.00	0.16	0.01	0.00	0.08
	2	0.17	0.07	0.16	0.18	0.02	0.00	0.15	0.00	0.16	0.01	0.08	0.00
	3	0.17	0.07	0.16	0.18	0.02	0.00	0.15	0.08	0.16	0.01	0.00	0.00
MR8	4	0.19	0.07	0.20	0.15	0.00	0.00	0.18	0.00	0.16	0.01	0.00	0.04
	5	0.21	0.00	0.18	0.00	0.00	0.18	0.24	0.00	0.14	0.01	0.04	0.00
	6	0.19	0.06	0.19	0.18	0.00	0.00	0.17	0.04	0.16	0.01	0.00	0.00
MR7	7	0.21	0.00	0.25	0.14	0.00	0.00	0.18	0.00	0.16	0.01	0.00	0.05
	8	0.21	0.00	0.24	0.18	0.00	0.00	0.18	0.00	0.14	0.01	0.04	0.00
	9	0.18	0.00	0.23	0.20	0.00	0.00	0.15	0.06	0.16	0.01	0.00	0.00
MR6	10	0.21	0.00	0.30	0.00	0.00	0.00	0.16	0.00	0.19	0.01	0.00	0.13
	11	0.21	0.00	0.23	0.25	0.00	0.00	0.11	0.00	0.19	0.01	0.00	0.00
	12	0.21	0.00	0.25	0.20	0.00	0.00	0.14	0.00	0.20	0.01	0.00	0.00
MR5	13	0.25	0.30	0.00	0.00	0.23	0.00	0.00	0.00	0.18	0.04	0.00	0.00
	14	0.25	0.32	0.00	0.00	0.23	0.00	0.00	0.00	0.18	0.02	0.00	0.00
	15	0.26	0.30	0.00	0.00	0.24	0.00	0.00	0.00	0.19	0.02	0.00	0.00

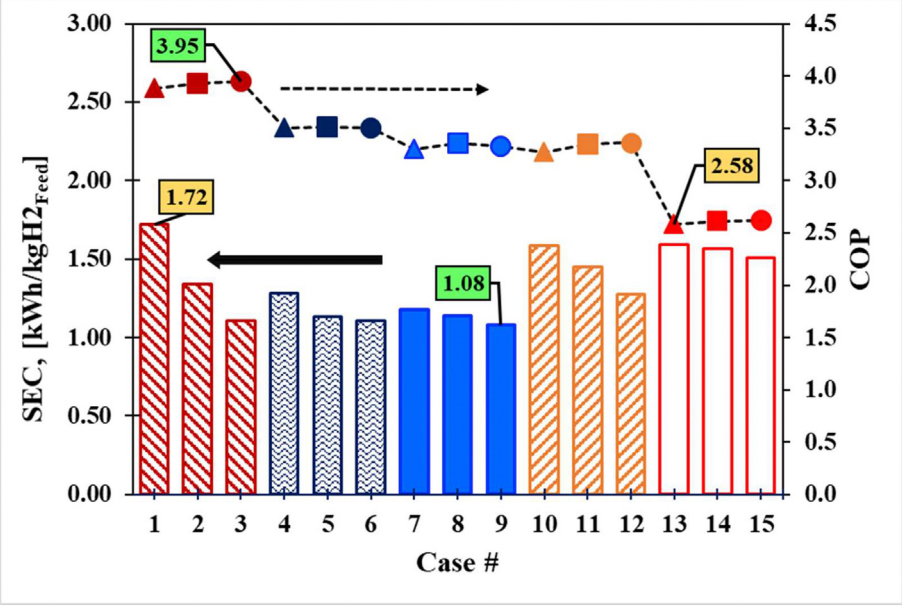

Fig. 4 – Total compression power and COP of the 15 mixed refrigerant cases.

require less MR flow rate to accomplish the HPP (See Appendix A, Table A1). However, P_h (22 bar) of the MR7 compositions is higher than that of MR9 (16 bar) and MR8 (20 bar). Higher P_h negatively affects the COP of the MR7 cases (3.3 as average) compared to that of MR8 (3.5) and MR9 (3.95), see Fig. 4. However, it yields better match between the hot and cold composite curves of MR7 (See Fig. 5, Case 7), which is the dominant factor in the reduction of the SEC.

For the quantitative analysis of the 15 cases presented in Table 2, it can be noted that the molar fraction of H_2 is only 1% of the MR in the most efficient cases (cases 3, 6, and 9) which is sufficient to achieve the target precooling temperature (−195 °C). A higher fraction of H_2 in the mixture increases the compression power with no improvement in the quantity of the evaporation capacity of HX3 and causes high SEC for cases 13, a4, and 15. For the fraction of C1, it is varying between 17% and 26% in the 15 MR cases. In the best performance cases, the fraction of C1 did not exceed 19% as the unnecessary increase of C1 maximize the compression power in a similar trend for H_2. For the C2 fraction, it is varying from 0% to 32% as shown in Table 2 with a fraction of less than 7% in the best cases. In particular, C2 forms 0% of the composition of Case 9, which is one of the best performance cases. However, the presence of C2 in the MR is needed for some mixtures (especially for five-component mixtures) to avoid the thermophysical problems (temperature-cross or overlapped, presented in Fig. 3) in the middle part of HX3. For C2*, its fraction forms 16%–30% in the first 12 cases and 0% in the rest cases. The presence of C2* is completive for C1 with less compression power and less compression power. So, if C2* is removed and substituted with lighter components (C1 or C2), higher compression power will be needed which yields higher SEC as shown for cases 13 to 15 in Fig. 4. Similar to C1, the presence of N_2 is essential and forms 14%–20% of the MR composition. However, the percent of N2 should be minimized to the least possible fraction as its compression consumes high energy

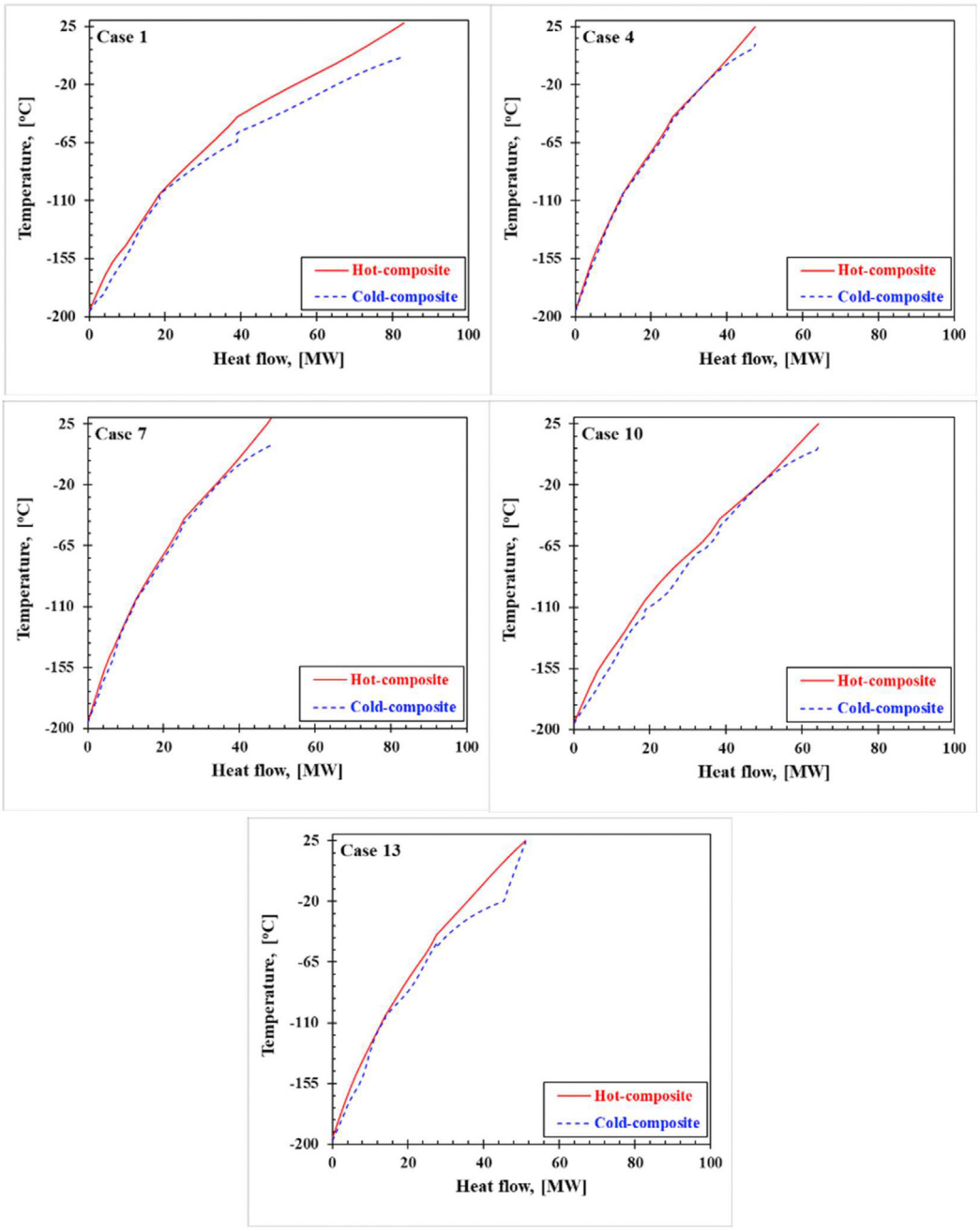

Fig. 5 – Composite curves of Case 1, Case 4, Case 7, Case 10, and Case 13. Note: the hot composite is pure hydrogen, and the cold composite is a mixed refrigerant, which is presented in Table 2 for each case.

close to that of hydrogen. Apart from the share of the lightweight components, C3 and n-C5 have the largest share as heavyweight components in the best performance cases with an average share of 19% and 16% of the MR, respectively. Thus, these components are recommended for the efficient performance of HX1 with less power consumption considering that the fraction of C3 should be minimized to the minimum possible value.

From the above results, it is found that the MR in Case 3, Case 6, and Case 9 have the best performance from an energetic point of view followed by Case 12. To have a close insight into the effect of the MR composition on the design of the MSHXs, the major properties of the vapor flows through the cold section of each heat exchanger are plotted for Case 3, Case 9, and Case 12 as presented in Fig. 6. On one hand, Case 9 has the minimum vapor flow and the highest cumulative overall heat transfer coefficient (UA) through HX1 and HX2 (see Fig. 6 (c, d), which is considered as a further advantage for this case from an economic point of view. The increase of the UA is caused by the increase of the heat transfer coefficient (U) with a constant heat transfer area (A). This implies that higher evaporation capacity could be obtained in Case 9 with the same heat transfer area as of Case 3 or Case 12. In addition, higher UA with a lower flow rate for

the MR minimizes the compression power, which is one of the key variables that need to be minimized to reduce the operational costs of the liquefaction system and enhance the economic features of the process [23]. On the other hand, as shown in Fig. 6 (a, b), Case 12 has the highest vapor Cp, the lowest vapor density, and the lowest UA in HX1 and HX3 compared to that of Case 3 and Case 9. This implies that larger heat exchangers are needed to be fit with the MR in Case 12. It should be noted that there is a phase transition of the lightweight components in the MR from the liquid phase into the vapor phase at the cold side of HX3. This implies that there are two phases (liquid and vapor) for each lightweight component (C1, C2, C2*, R14, N_2, and H_2) in HX3. Also, the locations at which the transition of the components from liquid to vapor phase occurs through the HX3 evaporator are not identical. Therefore, at the evaporator pressure in HX3 (2 bar) and over the temperature range of (−195 °C to 25 °C), the specific heat of some components continuously increases with the temperature such as H_2, or first increases then decreases as C1 and R14, or consciously decreases such as C2 and C2*. Thus, the curves of the Cp are fluctuating (Fig. 6 (a)) according to the nature of the specific heat of the involved components in the mixture. For the vapor density, it generally decreases with the increase of the temperature with a slight increase at the temperature range of (−145 °C to −110 °C) in Case 3 and Case 9 due to the presence of R14 that starts the evaporation process at −127 °C and has levelized density near its boiling temperature.

In conclusion, Case 9 (MR7) introduces superior performance in terms of SEC and compactness of the MSHXs compared to that of MR3 (MR9) and Case 12 (MR6). To ensure this result, further sensitivity analysis over a wide range of operating conditions must be conducted for the best five cases of the investigated compositions as presented in the next section.

Sensitivity analysis

After the development of the 15 MRs using the criteria and procedures developed in this study, the best five cases (Case 3, Case 6, Case 9, Case 12, and Case 15) are considered for further sensitivity analysis. This is a fundamental step to ensure that the operating conditions of the HPP are optimally selected for each case. Four major operating conditions (low-pressure P_l, higher-pressure P_h, target temperature T_4, and aftercooler temperature) are tested to examine their effects on the total compression power and MR flow rate of the HPP.

For the best-selected cases, the P_l of the HPP is changed from the design point value (2 bar) to within the range of 1 bar–5 bar as shown in Fig. 7. Ideally, as the P_l is increased, the compression duty of the compressor is reduced, and consequently, the compression power is decreased. However, in the HPP, as the P_l is increased from 2 bar to 5 bar, the compression power is increased for all cases (Fig. 7(a)). This is explained by that higher P_l reduces the refrigeration effect of the MR and a higher MR flow rate is needed to meet the same cooling load of the process (Fig. 7(b)). In contrast, as P_l is reduced to 1 bar, higher compression power is needed as the MR flow rate remains mostly the same as at 2 bar. Case 12 shows higher sensitivity for the increase of P_l as its compression power increased by 38% compared to less than 22% for the other cases.

For the high-pressure P_h effect, the five cases are simulated at a low-pressure of 2 bar with a P_h range of 12 bar–28 bar as shown in Fig. 8. It is noted that Case 15 shows the highest sensitivity for the variation of P_h. The major difference between Case 15 and other cases simulated in Fig. 8 is the high fraction of C2 in the MR composition (30%) which is five times higher than in Case 6 (6%) and about four times higher than in Case 3 (7%). In addition, Case 9 and Case 12 have zero fractions of C2. This implies that C2 causes poor performance for the HPP as it is a lightweight component with the least boiling point temperature compared to the other lightweight components (See Table 1). As C2* gives a better match in the composite curves of the MSHXs than C2 as shown in Fig. 5 (Case 10 with C2*, Case 13 with C2). Therefore, it is recommended to replace the fraction of C2 with C2* to improve the MR performance in the HPP. Despite the behavior of Case 15, the other cases show optimal performance at P_h of 20 bar at which the minimum MR flow is achieved (see Fig. 8(b)).

The cooling process of the MR at intermediate and high pressures plays a key role in the compression power and the distribution of the MR flow through the MSHXs. For instance, if the cooling process is carried out at low temperatures (20 °C–30 °C) using water (wet-cooling), the liquid-phase fraction at stream 7 (Fig. 1) will be more than if conducted at higher temperatures (35 °C–40 °C) using air (dry-cooling). This means that a higher portion of the MR flow will be pressurized to P_h through the pump rather than Com-2, which significantly reduces the total compression power of the process. Fig. 9 depicts how the compression power and the MR flow change with the increase of the aftercooler temperature from the wet-cooling range to the dry-cooling range. The most important result here is that Case 6 shows the least sensitivity for the aftercooler temperature. Unlike other cases, the MR flow of Case 6 only increased by 7% as the aftercooler temperature increased from 20 °C (86 kg/s) to 40 °C (92 kg/s).

Another important result in Fig. 9 is the behavior of Case 9, which has the minimum SEC over other cases. Case 9 requires MR flow at 25 °C lower than at 20 °C (Fig. 9(b)) with a negligible increase in the compression power (less than 0.52%). This is explained by that for Case 9, aftercooler temperature less than 25 °C reduces the portion of the lightweight components in HX2 and HX3, which dictates a higher flow rate to avoid temperature-cross or overlapped issues in these heat exchangers. From the above results, it can be stated that Case 9 has the minimum SEC (1.08 kWh/kg$H2_{Feed}$) at an aftercooler temperature of 25 °C compared to 1.11 kWh/kg$H2_{Feed}$ for Case 6 at the same temperature. However, Case 6 has the lowest compression power with SEC of 1.32 kWh/kg$H2_{Feed}$ at aftercooler temperature higher than 37 °C compared to 1.45 kWh/kg$H2_{Feed}$ for Case 9. Therefore, Case 9 is recommended for the wet-cooling conditions and Case 6 for the dry-cooling conditions. But, even though the wet-conditions yield lower SEC than dry-conditions, the capital and operational costs of the wet-cooling system are higher than of the dry-cooling system [43,44]. Therefore, for accurate decision for the selection of the wet or dry cooling

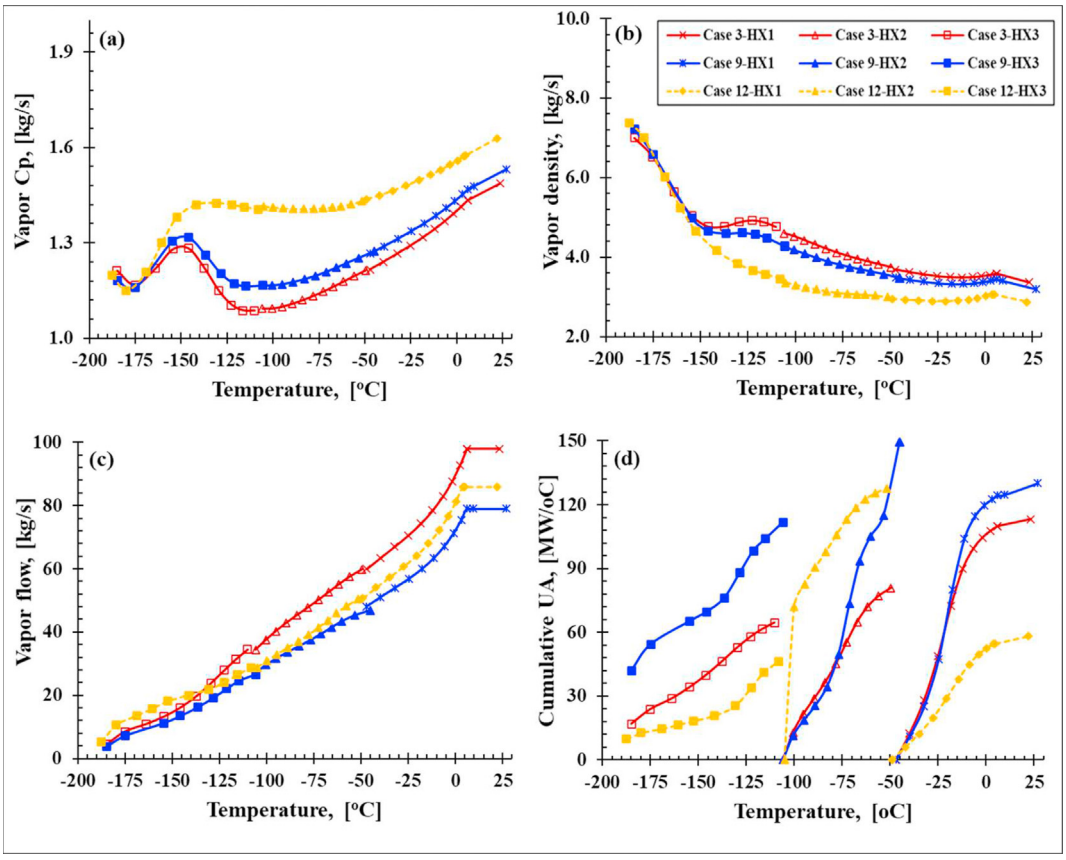

Fig. 6 – Variation the (a) vapor specific heat, (b) vapor density, (c) vapor flow rate, and (d) cumulative heat transfer coefficient of cases 3, 9, and 12 through HX1, HX2, and HX3.

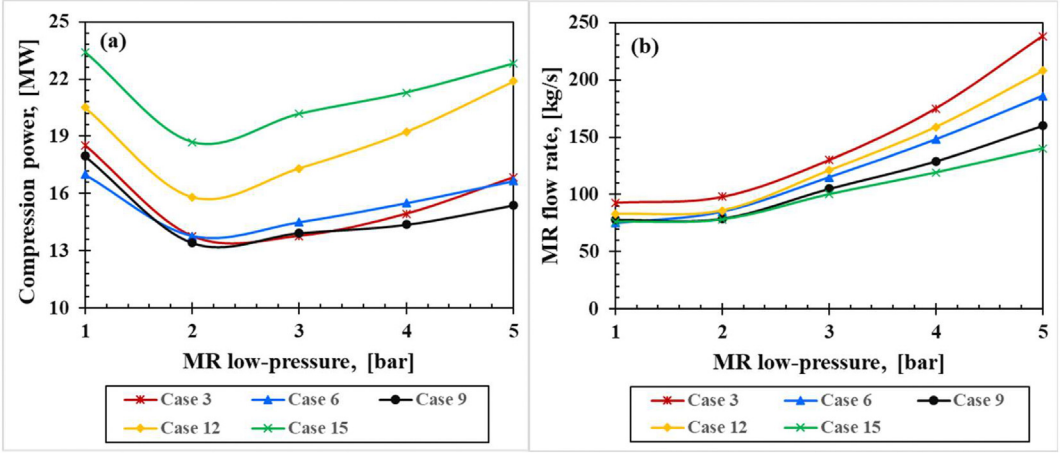

Fig. 7 – Effect of the MR low-pressure on the process (a) compression power, and (b) MR flow rate.

conditions, further economic assessment is needed for each situation and is recommended as a future work.

Composition sensitivity and comparisons

As Case 6 shows competitive performance for Case 9 at wet-cooling conditions and the best performance at the dry-cooling conditions, it is considered here for further analysis by optimizing its MR composition. This is done by keeping the single components of MR in Case 6 with further modifications for their proportions as shown in Fig. 10. Two optimization scenarios are presented in Fig. 10, referred to as Case 6-S1, and Case 6-S2, respectively. In Case 6-S1, the fraction of C2 is significantly reduced from 6% to 1.97% with a parallel increase in the fraction of R14 from 4.00% to 8.28%. This mitigates the negative impact of C2 on the SEC and improves the refrigeration effect of the mixture. This resulted in decreasing the SEC from 1.11 kWh/kgH2$_{Feed}$ in Case 6-Basic to 1.07 kWh/kgH2$_{Feed}$

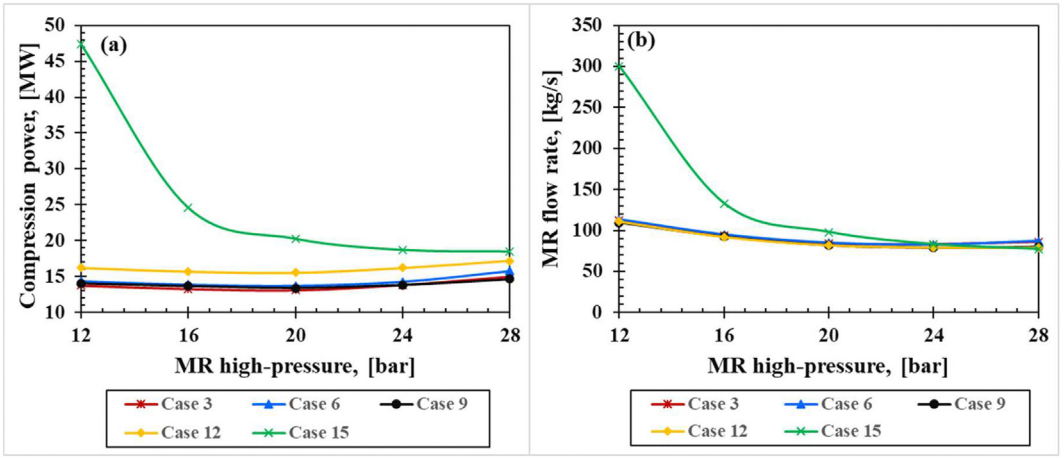

Fig. 8 – Effect of the MR high-pressure on the process (a) compression power, and (b) MR flow rate.

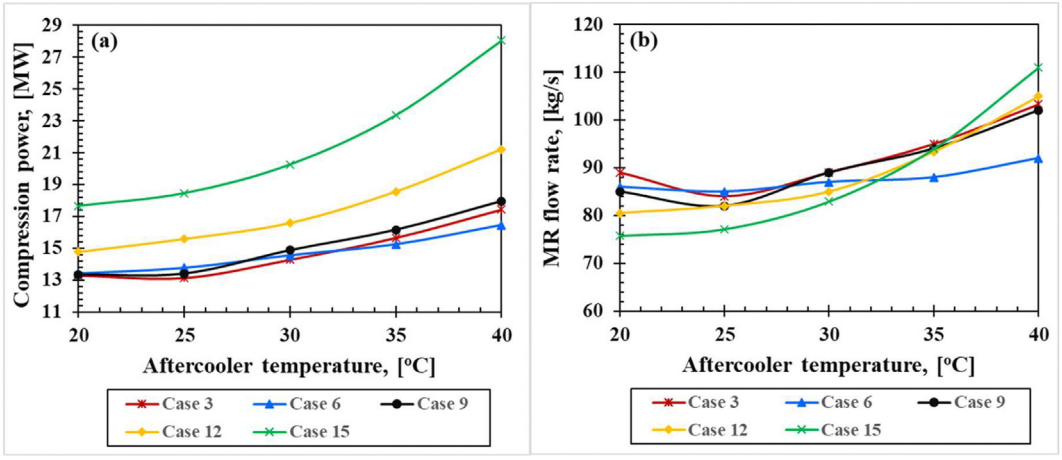

Fig. 9 – Effect of the aftercooler temperature on the process (a) compression power, and (b) MR flow rate.

in Case 6-S1 (reduced by 3.60%). In Case 6-S2, the component fractions were further tuned with notable reduction for the fraction of H_2 from 1.42% to only 0.2%. Consequently, the SEC is reduced to 1.03 kWh/kgH2$_{Feed}$, which is 7.21% lower than Case b-Basic, and 3.74% lower than Case 6-S1.

From the sensitivity analysis, it is found that the MR composition in Case 9 has the minimum SEC (1.08 kWh/kgH2$_{Feed}$) at an aftercooler temperature of 25 °C. However, the optimized composition of Case 6-S2 yields 1.03 kWh/kgH2$_{Feed}$ (4.63 lower than Case 9) at the same aftercooler temperature. Taking into account that Case 6 has superior performance at dry-conditions, Case 6-S2 can be recommended for the HPP at both wet and dry cooling conditions.

To reveal the features of the new optimized MR composition of Case 6-S2, the characteristics of four reference processes (referred to as RC1, RC2, RC3, and RC4) available in the literature were compared as shown in Table 3. The detailed composition of the MR of each process is reported in Table 3 and schematically presented in Fig. 11. On one hand, although both RC1 and RC4 have a nine-component mixture (MR9), RC1 has higher capacity (87 TPD) and lower target temperature (−198 °C) than RC4 (54 TPD, −195 °C). But, RC4 has used H_2 instead of Neon for the cryogenic section in HX3. Therefore, the SEC of RC4 is 45.73% lower than of RC1. On the other hand, both RC2 and RC3 have the same capacity (100 TPD) and the same target temperature (−198 °C). Although RC2 has eleven-component mixture (MR11), its SEC is 12% higher than RC3. This is caused by two reasons: (1) the presence of NH_3 and propene (C3*) in the MR of RC2, (2) the portion of the heavyweight components is larger than of the lightweight components, which yield a poor match for the composite curves of HX2 and HX3 of the process.

Comparing the MR composition of Case 6-S2 (MR8) presented in this study with the four reference processes, it can be noted that there is no Neon, NH_3, or C3* in the mixture with the smallest fraction of C2. Also, the lightweight portion (63) is larger than the heavyweight components (37%). In addition, the capacity of the HPP with Case 6-S2 is 300 TPD, which is about three to four times higher than of all reference processes at a target temperature of −198 °C. For these reasons, the SEC of Case 6-S2 is 49.78% lower than of RC1, 35.14% lower than of RC2, 27.26% lower than of RC3, and 7.46% lower than of

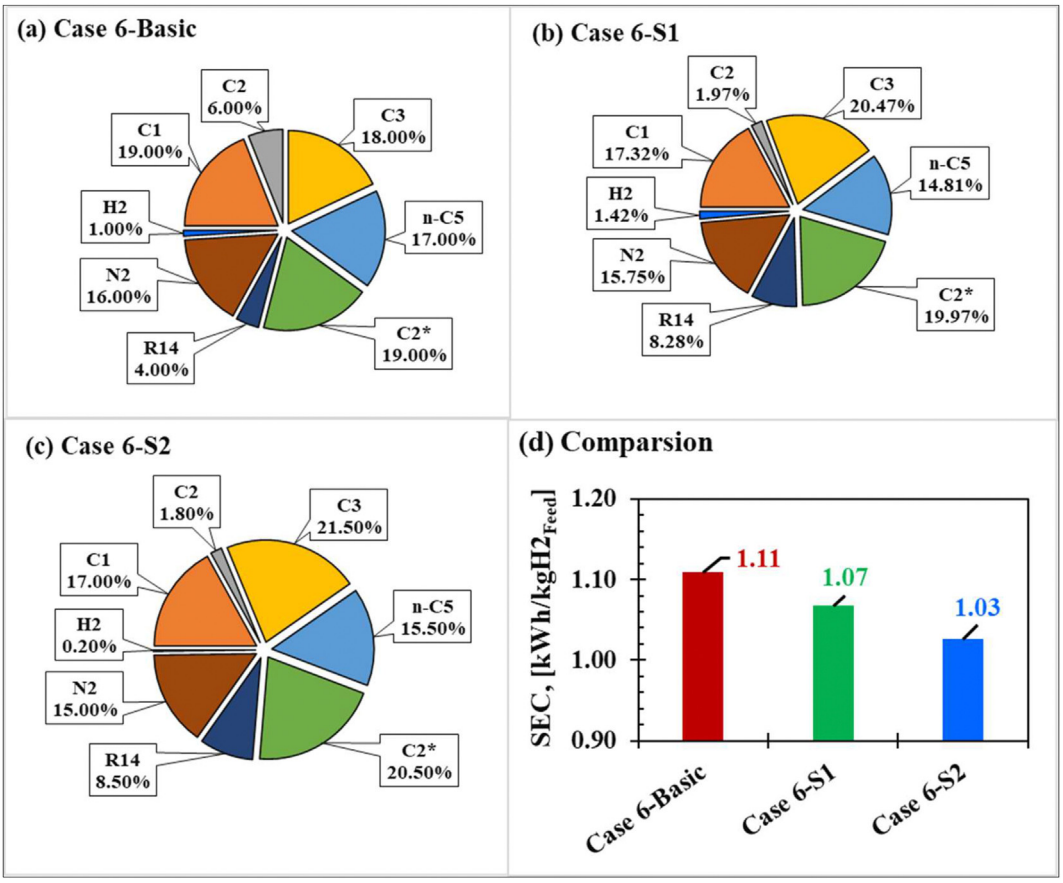

Fig. 10 – Results of optimizing the MR composition presented in Case 6. (a) Basic composition, (b) first scenario of optimized composition, and (c) second scenario of optimized composition.

Table 3 – Comparison between hydrogen precooling processes available in the literature with the present process at the optimal MR composition Case 6-S2.

Reference		RC1 [1]	RC2 [2]	RC3 [3]	RC4 [4]	Present study (Case 6-S2)
Process capacity, [MTD]		87	100	100	54	300
Target temperature T_4, [°C]		−198	−198	−198	−195	−198
Category		MR9	MR11	MR5	MR9	MR8
SEC, [kWh/kgH2$_{Feed}$]		2.051	1.588	1.416	1.113	1.030
MR molar-based composition, (%)	Methane (C1)	16.60	10.20	24.00	11.30	17.00
	Ethane (C2)	8.60	19.25	28.00	5.67	1.80
	Ethylene (C2*)	11.80	0.00	0.00	12.15	20.50
	Propane (C3)	19.40	5.32	0.00	19.92	21.50
	i-Butane (i-C4)	0.00	2.43	0.00	3.18	0.00
	n-Butane (n-C4)	6.60	2.35	26.00	0.00	0.00
	n-Pentane (n-C5)	11.80	29.82	0.00	31.46	15.50
	Refrig-14 (R14)	7.20	9.86	0.00	5.51	8.50
	Nitrogen (N_2)	15.60	6.42	18.00	10.21	15.00
	Hydrogen (H_2)	0.00	0.02	4.00	0.63	0.20
	Neon (Ne)	2.40	0.00	0.00	0.00	0.00
	Propene (C3*)	0.00	12.73	0.00	0.00	0.00
	Ammonia (NH_3)	0.00	1.58	0.00	0.00	0.00

RC4. More importantly, the SEC of Case 6-S2 (1.03 kWh/kgH2$_{Feed}$) is much lower than of the commercial HPPs available in the industrial sector. For instance, the SEC of the HPP at Ingolstadt is 4.86 kWh/kgH2$_{Feed}$, about five times higher than of Case 6-S2.

Despite that the optimized case (Case 6-S2) showed best SEC performance, all the 15 MR cases presented in this study have SEC lower than of RC1 in Table 3. Moreover, the SEC of MR8 and MR7 groups are lower than that of RC2 and RC3. This confirms that, by applying the systematic approach developed

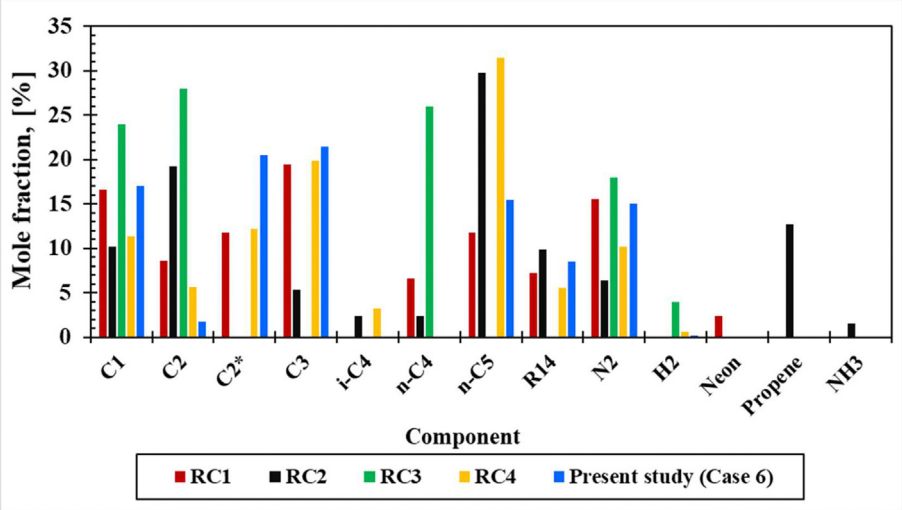

Fig. 11 – Schematic presentation of the MR composition in the reference cases (RC1, RC2, RC3, and RC4) compared to that of Case 6 in the present study.

in this study to design a MR for the HPP, an energy-efficient HPP at various operating conditions (e.g., wet, and dry cooling, large capacities, and very low cryogenic temperature) can be obtained. With additional sensitivity and optimization analysis, the SEC can be reduced to extremely lower values than of the processes available in the literature.

Conclusions

In this study, a thermodynamic systematic approach for the design of a mixed refrigerant (MR) for the hydrogen precooling process (HPP) is developed. The developed approach is composed of four criteria as guidelines for the initial selection of the candidate refrigerants. Then, detailed procedures to develop an optimal MR are discussed through seven major steps. The developed approach was tested by creating new 15 mixed refrigerants for the HPP with various compositions and proportions. The 15 MRs (referred to as cases) were divided into five groups, based on the number of the single components in each mixture. These groups contain nine-component (MR9), eight-component (MR8), seven-component (MR7), six-component (MR6), and five-components (MR5) based mixtures. The new compositions are analyzed from an energy point of view using the specific energy consumption (SEC) and coefficient of performance (COP) as the performance indicators of the HPP. Then, further sensitivity and optimization analyses are performed to improve the performance of the HPP by obtaining the optimal SEC for each MR. Among the 15 investigated cases, it is found that:

- The candidate refrigerants must be divided into lightweight and heavyweight refrigerants based on the boiling point temperature.
- For the HPP with a target temperature less than −193 °C, it is recommended to set the total portion of the lightweight components larger than the heavyweight portions.
- Eight-component MR (MR8) is the best option to create an optimal mixture for the cryogenic cooling process with a sufficient match between the composite curves of all heat exchangers of the HPP.
- The presence of methane (C1), nitrogen (N_2), and hydrogen (H_2) components are essential to achieve an energy-efficient HPP.
- The use of ethylene (C2*) instead of ethane (C2), H2 instead of neon, and R14 instead of NH3 is recommended to optimize the SEC of the HPP.
- At an aftercooler temperature of 25 °C (wet-cooling), MR in Case 9 is recommended, while at an aftercooler temperature of 40 °C (dry-cooling), MR in Case 6 is recommended.

Finally, optimizing the MR composition of Case 6 reduces the SEC to 1.03 kWh/kh$H2_{Feed}$, which is lower than the SEC of all HPPs reported in literature. However, further robust optimization analysis for the entire 15 MR cases with further exergoeconomic assessment is recommended for future work.

CRediT author statement

Ahmad K. Sleiti: Conceptualization, Investigation, Writing-Original Draft, Review & Editing, Resources, Formal analysis, Project administration, Funding acquisition, Supervision. **Wahib A. Al-Ammari:** Conceptualization, Writing-Original Draft, Investigation, Software, Data Curation, Validation, Formal analysis.

Declaration of competing interest

The authors declare that they have no known competing financial interests or personal relationships that could have appeared to influence the work reported in this paper.

Acknowledgement

The work presented in this publication was made possible by NPRP-S grant # [11S-1231-170155] from the Qatar National Research Fund (a member of Qatar Foundation). The findings herein reflect the work, and are solely the responsibility, of the authors.

Appendix A. Supplementary data

Supplementary data to this article can be found online at https://doi.org/10.1016/j.ijhydene.2022.04.233.

REFERENCES

[1] Lebrouhi BE, Djoupo JJ, Lamrani B, Benabdelaziz K, Kousksou T. Global hydrogen development - a technological and geopolitical overview. Int J Hydrogen Energy 2022;47:7016–48. https://doi.org/10.1016/j.ijhydene.2021.12.076.

[2] Yukesh Kannah R, Kavitha S, Preethi, Parthiba Karthikeyan O, Kumar G, Dai-Viet NV, et al. Techno-economic assessment of various hydrogen production methods – a review. Bioresour Technol 2021;319:124175. https://doi.org/10.1016/j.biortech.2020.124175.

[3] Ishimoto Y, Voldsund M, Nekså P, Roussanaly S, Berstad D, Gardarsdottir SO. Large-scale production and transport of hydrogen from Norway to Europe and Japan: value chain analysis and comparison of liquid hydrogen and ammonia as energy carriers. Int J Hydrogen Energy 2020;45:32865–83. https://doi.org/10.1016/j.ijhydene.2020.09.017.

[4] Okunlola A, Giwa T, Di Lullo G, Davis M, Gemechu E, Kumar A. Techno-economic assessment of low-carbon hydrogen export from western Canada to eastern Canada, the USA, the asia-pacific, and europe. Int J Hydrogen Energy 2022;47:6453–77. https://doi.org/10.1016/j.ijhydene.2021.12.025.

[5] Ratnakar RR, Gupta N, Zhang K, van Doorne C, Fesmire J, Dindoruk B, et al. Hydrogen supply chain and challenges in large-scale LH2 storage and transportation. Int J Hydrogen Energy 2021;46:24149–68. https://doi.org/10.1016/j.ijhydene.2021.05.025.

[6] Jackson S, Brodal E. Optimization of the energy consumption of a carbon capture and sequestration related carbon dioxide compression processes. Energies 2019;12. https://doi.org/10.3390/en12091603.

[7] Franco BA, Baptista P, Neto RC, Ganilha S. Assessment of offloading pathways for wind-powered offshore hydrogen production: energy and economic analysis. Appl Energy 2021;286. https://doi.org/10.1016/j.apenergy.2021.116553.

[8] Razi F, Dincer I. Challenges, opportunities and future directions in hydrogen sector development in Canada. Int J Hydrogen Energy 2022;47:9083–102. https://doi.org/10.1016/j.ijhydene.2022.01.014.

[9] Bi Y, Yin L, He T, Ju Y. Optimization and analysis of a novel hydrogen liquefaction process for circulating hydrogen refrigeration. Int J Hydrogen Energy 2021;47:348–64. https://doi.org/10.1016/j.ijhydene.2021.10.012.

[10] Hjeij D, Biçer Y, Koç M. Hydrogen strategy as an energy transition and economic transformation avenue for natural gas exporting countries: Qatar as a case study. Int J Hydrogen Energy 2022;47:4977–5009. https://doi.org/10.1016/j.ijhydene.2021.11.151.

[11] Nazir H, Louis C, Jose S, Prakash J, Muthuswamy N, Buan MEM, et al. Is the H2 economy realizable in the foreseeable future? Part I: H2 production methods. Int J Hydrogen Energy 2020;45:13777–88. https://doi.org/10.1016/j.ijhydene.2020.03.092.

[12] He T, Karimi IA, Ju Y. Review on the design and optimization of natural gas liquefaction processes for onshore and offshore applications. Chem Eng Res Des 2018;132:89–114. https://doi.org/10.1016/j.cherd.2018.01.002.

[13] Nazir H, Muthuswamy N, Louis C, Jose S, Prakash J, Buan ME, et al. Is the H2 economy realizable in the foreseeable future? Part II: H2 storage, transportation, and distribution. Int J Hydrogen Energy 2020;45:20693–708. https://doi.org/10.1016/j.ijhydene.2020.05.241.

[14] Nazir H, Muthuswamy N, Louis C, Jose S, Prakash J, Buan MEM, et al. Is the H2 economy realizable in the foreseeable future? Part III: H2 usage technologies, applications, and challenges and opportunities. Int J Hydrogen Energy 2020;45:28217–39. https://doi.org/10.1016/j.ijhydene.2020.07.256.

[15] Naquash A, Qyyum MA, Islam M, Sial NR, Min S, Lee S, et al. Performance enhancement of hydrogen liquefaction process via absorption refrigeration and organic Rankine cycle-assisted liquid air energy system. Energy Convers Manag 2022;254:115200. https://doi.org/10.1016/j.enconman.2021.115200.

[16] Cao Y, Dhahad HA, Togun H, Aly AA, Felemban BF, El-Shafay AS, et al. Application, comparative study, and multi-objective optimization of a hydrogen liquefaction system utilizing either ORC or an absorption power cycle. Int J Hydrogen Energy 2021. https://doi.org/10.1016/j.ijhydene.2021.11.191. In press.

[17] Jouybari AK, Ilinca A, Ghorbani B, Rooholamini S. Thermodynamic and exergy evaluation of an innovative hydrogen liquefaction structure based on ejector-compression refrigeration unit, cascade multi-component refrigerant system, and Kalina power plant. Int J Hydrogen Energy 2022:1–25. https://doi.org/10.1016/j.ijhydene.2022.01.190.

[18] Karimi M, Mehrpooya M, pourfayaz F. Proposal and investigation of a novel hybrid hydrogen production and liquefaction process using solid oxide electrolyzer, solar energy, and thermoelectric generator. J Clean Prod 2022;331:130001. https://doi.org/10.1016/j.jclepro.2021.130001.

[19] Ghorbani B, Zendehboudi S, Moradi M. Development of an integrated structure of hydrogen and oxygen liquefaction cycle using wind turbines, Kalina power generation cycle, and electrolyzer. Energy 2021;221:119653. https://doi.org/10.1016/j.energy.2020.119653.

[20] Naquash A, Riaz A, Lee H, Qyyum MA, Lee S, Lam SS, et al. Hydrofluoroolefin-based mixed refrigerant for enhanced performance of hydrogen liquefaction process. Int J Hydrogen Energy 2022:1–15. https://doi.org/10.1016/j.ijhydene.2022.02.010.

[21] Yin L, Ju Y. Review on the design and optimization of hydrogen liquefaction processes. Front Energy 2020;14:530–44. https://doi.org/10.1007/s11708-019-0657-4.

[22] Zhang S, Liu G. Design and performance analysis of a hydrogen liquefaction process. Clean Technol Environ Policy 2022;24:51–65. https://doi.org/10.1007/s10098-021-02078-z.

[23] Bian J, Yang J, Li Y, Chen Z, Liang F, Cao X. Thermodynamic and economic analysis of a novel hydrogen liquefaction process with LNG precooling and dual-pressure Brayton cycle. Energy Convers Manag 2021;250:114904. https://doi.org/10.1016/j.enconman.2021.114904.

[24] Garceau NM, Baik JH, Lim CM, Kim SY, Oh IH, Karng SW. Development of a small-scale hydrogen liquefaction system.

Int J Hydrogen Energy 2015;40:11872–8. https://doi.org/10.1016/j.ijhydene.2015.06.135.
[25] Yin L, Ju Y. Process optimization and analysis of a novel hydrogen liquefaction cycle. Int J Refrig 2020;110:219–30. https://doi.org/10.1016/j.ijrefrig.2019.11.004.
[26] Yuksel YE, Ozturk M, Dincer I. Analysis and assessment of a novel hydrogen liquefaction process. Int J Hydrogen Energy 2017;42:11429–38. https://doi.org/10.1016/j.ijhydene.2017.03.064.
[27] Incer-Valverde J, Mörsdorf J, Morosuk T, Tsatsaronis G. Power-to-liquid hydrogen: exergy-based evaluation of a large-scale system. Int J Hydrogen Energy 2021. https://doi.org/10.1016/j.ijhydene.2021.09.026. In press.
[28] Bae JE, Wilailak S, Yang JH, Yun DY, Zahid U, Lee CJ. Multi-objective optimization of hydrogen liquefaction process integrated with liquefied natural gas system. Energy Convers Manag 2021;231:113835. https://doi.org/10.1016/j.enconman.2021.113835.
[29] Faramarzi S, Nainiyan SMM, Mafi M, Ghasemiasl R. A novel hydrogen liquefaction process based on LNG cold energy and mixed refrigerant cycle. Int J Refrig 2021;131:263–74. https://doi.org/10.1016/j.ijrefrig.2021.07.022.
[30] Chang H-M, Gyun Park M. Cascade JT Systems with single-component refrigerants for hydrogen liquefaction. Cryogenics 2021;121:103410. https://doi.org/10.1016/j.cryogenics.2021.103410.
[31] Naquash A, Qyyum MA, Min S, Lee S, Lee M. Carbon-dioxide-precooled hydrogen liquefaction process: an innovative approach for performance enhancement–Energy, exergy, and economic perspectives. Energy Convers Manag 2022;251:114947. https://doi.org/10.1016/j.enconman.2021.114947.
[32] Ghorbani B, Mehrpooya M, Amidpour M. A novel integrated structure of hydrogen purification and liquefaction using natural gas steam reforming, organic Rankine cycle and photovoltaic panels. Cryogenics 2021;119:103352. https://doi.org/10.1016/j.cryogenics.2021.103352.
[33] Krasae-In S. Optimal operation of a large-scale liquid hydrogen plant utilizing mixed fluid refrigeration system. Int J Hydrogen Energy 2014;39:7015–29. https://doi.org/10.1016/j.ijhydene.2014.02.046.
[34] Asadnia M, Mehrpooya M. A novel hydrogen liquefaction process configuration with combined mixed refrigerant systems. Int J Hydrogen Energy 2017;42:15564–85. https://doi.org/10.1016/j.ijhydene.2017.04.260.
[35] Cardella U, Decker L, Sundberg J, Klein H. Process optimization for large-scale hydrogen liquefaction. Int J Hydrogen Energy 2017;42:12339–54. https://doi.org/10.1016/j.ijhydene.2017.03.167.
[36] Berstad DO, Stang JH, Nekså P. Large-scale hydrogen liquefier utilising mixed-refrigerant pre-cooling. Int J Hydrogen Energy 2010;35:4512–23. https://doi.org/10.1016/j.ijhydene.2010.02.001.
[37] Sadaghiani MS, Mehrpooya M. Introducing and energy analysis of a novel cryogenic hydrogen liquefaction process configuration. Int J Hydrogen Energy 2017;42:6033–50. https://doi.org/10.1016/j.ijhydene.2017.01.136.
[38] Krasae-in S, Stang JH, Neksa P. Development of large-scale hydrogen liquefaction processes from 1898 to 2009. Int J Hydrogen Energy 2010;35:4524–33. https://doi.org/10.1016/j.ijhydene.2010.02.109.
[39] Krasae-In S, Stang JH, Neksa P. Simulation on a proposed large-scale liquid hydrogen plant using a multi-component refrigerant refrigeration system. Int J Hydrogen Energy 2010;35:12531–44. https://doi.org/10.1016/j.ijhydene.2010.08.062.
[40] Sleiti AK. Isobaric expansion engines powered by low-grade heat—working fluid performance and selection database for power and thermomechanical refrigeration. Energy Technol 2020;8:2000613. https://doi.org/10.1002/ente.202000613.
[41] Sleiti AK, Al-Ammaria WA, Al-Khawaja M, Karbon M, Al-Ammari WA. A combined thermo-mechanical refrigeration system with isobaric expander-compressor unit powered by low grade heat – design and analysis. Int J Refrig 2020;120:39–49. https://doi.org/10.1016/j.ijrefrig.2020.08.017.
[42] Berstad D, Skaugen G, Wilhelmsen Ø. Dissecting the exergy balance of a hydrogen liquefier: analysis of a scaled-up claude hydrogen liquefier with mixed refrigerant pre-cooling. Int J Hydrogen Energy 2021;46:8014–29. https://doi.org/10.1016/j.ijhydene.2020.09.188.
[43] Sleiti AK, Al-Ammari WA, Vesely L, Kapat JS. Thermoeconomic and optimization analyses of direct oxy-combustion supercritical carbon dioxide power cycles with dry and wet cooling. Energy Convers Manag 2021;245:114607. https://doi.org/10.1016/j.enconman.2021.114607.
[44] Sleiti AK, Al-Ammari WA, Aboueata KM. Flare gas-to-power by direct intercooled oxy-combustion supercritical CO2 power cycles. Fuel 2022;308:121808. https://doi.org/10.1016/j.fuel.2021.121808.